IEEE Journal of Microwaves

Received 7 June 2022; revised 5 August 2022 and 23 September 2022; accepted 29 September 2022.

Digital Object Identifier 10.1109/JMW.2022.3211428

Improved TM Dual-Mode Filters With Reduced Fabrication Complexity

CHAD BARTLETT [1] (Graduate Student Member, IEEE), JENS BORNEMANN [2] (Life Fellow, IEEE), AND MICHAEL HÖFT [1] (Senior Member, IEEE)

(Regular Paper)

[1]Institute of Electrical and Information Engineering, University of Kiel, 24143 Kiel, Germany
[2]Department of Electrical and Computer Engineering, University of Victoria, Victoria, BC V8W 2Y2, Canada

CORRESPONDING AUTHOR: Chad Bartlett (e-mail: chb@tf.uni-kiel.de).

This work was supported in part by European Union's Horizon 2020 Research and Innovation Programme under the Marie Słodowska-Curie Grant 811232-H2020-MSCA-ITN-2018 and in part by the DFG Open Access Publication Funding Programme of Kiel University.

ABSTRACT This work presents an alternate and improved approach for the design of dual-mode filters that utilize transverse magnetic (TM) and nonresonating modes. The method that is proposed in this work allows for an improvement of the typical TM dual-mode filter design through the reformation of the coupling irises that connect the TM dual-mode cavity to the source/load waveguide ports, where the new interconnection means takes the form of resonate slot-irises. In this manner, a fourth-order quasi-elliptic response can be achieved within a very limited physical geometry and able to cover more than double the usable fractional bandwidth than previously reported. Furthermore, the selectivity and insertion loss of the filter response is significantly improved when compared to the typical single-cavity TM dual-mode filter response that uses coupling irises, while on the comparison of equal-order structures, a reduction in fabrication complexity and improved insertion loss is achieved. A characterization of the dimensional variations and effects of altering one of the source/load port positions in the proposed filter design is investigated in order to demonstrate notable effects on the rejection characteristics and positions of transmission zeros. A presentation on the design theory is given and formulations of various filter responses are examined. The fabrication of an experimental prototype with approximately 7.3% fractional bandwidth (FBW), centered at 90 GHz is conducted using high-precision computer numerical control (CNC) milling in order to demonstrate that the unique simplicity and overall compaction of this method can be easily applied at millimetre-wave frequencies without the need of tuning means. The results which are presented demonstrate highly accurate measurements throughout the W-band range, while an additional Q-factor analysis is provided in order to compare the improved filter scheme with other known design methodologies.

INDEX TERMS Bandpass filter, dual-mode, millimetre-wave, miniaturization techniques, nonresonating modes, passive components, TM-mode, resonant-iris, waveguide filter, W-band.

I. INTRODUCTION

As waveguide technology remains the dominant choice in industry due to its performance capabilities, high-end communication and space-bound systems require constant adaptation of both the electrical and physical properties to meet the stringent conditions imposed by industry as well as meet the needs of future applications that call for the use of higher frequency ranges. For decades, solutions for innate, yet critical properties such as size and weight have been an important area of research and have resulted in many compact multi-mode or multi-band solutions. In the case of multi-mode designs, many versatile methods, such as [1], [2], [3], [4], [5], have been proposed that allow for compact and light-weight microwave filters to be developed for high-end applications. One of the most resourceful methods of accomplishing this has been through the adoption of nonresonating nodes (NRN) and nonresonating modes (NRM) in order to connect resonators more flexibly or allocate new bypass couplings throughout the

structure; several advanced examples can be reviewed in [5], [6], [7], [8], [9], [10], [11], [12], where new classes of highly-compact filter components that utilize transverse magnetic (TM) mode cavities are demonstrated. The use of TM-mode filters with nonresonating modes has driven much innovation and research into modular building-block designs and have allowed for many new filter structures to be demonstrated, for example [13], [14], [15], [16], [17], [18], [19].

Maximizing the capabilities of filter structures that have highly stringent requirements is of great interest but also comes with great difficulty. In examples such as [6], [11], [20], [21], [22], [23], [24], [25], resonating irises (RIs) have been proposed as a means of maximizing the use of given filter structures for single-band or dual-band configurations. It is clear that the impact of these types of resonating irises can have a significant influence not only on the obtainable filtering characteristics, but also the resulting size and weight. In light of these results, the use of resonating iris configurations in the literature is relatively low. Pushing these types of filters to their maximum potential is of great interest and can grant design engineers the ability to utilize all of the cavities and interconnecting irises with a minimum of two purposes or modes during operation.

To this end, we propose an improved configuration to the TM dual-mode filters presented by [8], [9], [10], where the general operation and geometric simplicity of the filter is further maximized through the inclusion of resonating irises at the source/load positions of the dual-mode cavity. A description of the configuration and the subsequent impact on dimensional variations are exhibited for the first time. The impact of this work demonstrates: a more than doubling of the usable fractional bandwidth, an increase in selectivity, an increase in filter order, and improved Q-factor, all with minimal alterations to the original work proposed in [8], [9], [10] when comparing characteristics of designs with single resonators and iris/slot-irises. Furthermore, -notwithstanding the aforementioned attributes- when considering a comparison of equal-order designs, a substantial reduction in fabrication complexity can be obtained while attaining a significantly improved Q-factor. An experimental prototype of a filter is constructed for W-band (75–110 GHz) operation in order to demonstrate the geometrical simplicity and elegance for micro-scale design where each elementary structure of the filter operates with at least two purposes, (e.i., the resonant slot-irises for main-line coupling and producing passband poles, and the TM dual-mode cavity for producing two poles and a nonresonating mode for bypass coupling). The experimental prototype is specified for a fractional bandwidth (FBW) of approximately 7.3% and centered at 90 GHz in order to demonstrate the unique simplicity and low geometric complexity of the design for millimetre-wave operations where alignment becomes highly critical and tuning means become impractical or infeasible. A comparison of the proposed filter design and other TM-mode filter solutions is provided in order to highlight the benefits of the new design methodology.

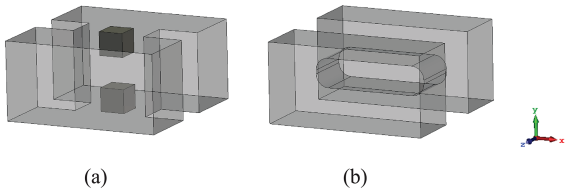

FIGURE 1. Equivalent evanescent-mode resonators fed by WR-10 waveguides; in (a) double-ridge form and (b) slot-iris form.

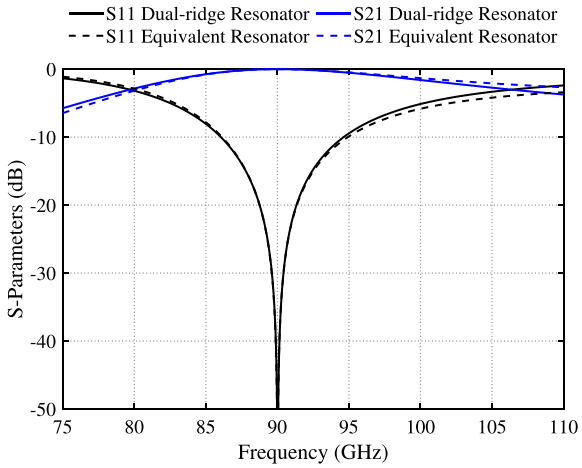

FIGURE 2. Simulated S-parameter results for the comparison of the double-ridge resonator and its equivalent slot-iris type resonator from Fig. 1.

II. RESONANT-IRIS APERTURES

Elementary resonating-irises can be configured from the general dimensions of a mixed-coupled (inductive and capacitive) slot-iris, or in the form of evanescent-mode partial-height posts (e.g., double ridge). Although evanescent-mode post-type designs have been utilized in work such as [11], the small and intricate details of partial-height posts make it difficult or even infeasible for the overall component to be scaled for millimetre and sub-millimetre wave applications. However, this partial-height post structure can be altered to form a synonymous configuration that avoids the use of partial-height posts and significantly eases fabrication. Fig. 1(a) depicts an evanescent-mode double-ridge resonant iris, while Fig. 1(b) depicts an equivalent form in the shape of a slot-type resonant iris. A comparison of the simulated S-parameter characteristics of both of these circuits is shown in Fig. 2 over the full W-band range, where the poles have been specified for 90 GHz operation. This demonstration instantiates a very similar behaviour over the full frequency band of interest for both the S_{11} and S_{21} response, and provides a suitable alternative to the manufacturing of partial-height post configurations in high-frequency applications. As a further demonstration, two interconnected resonating slot-irises are shown in Fig. 3 where the S-parameter responses for a variety of dimensional configurations are demonstrated in Fig. 4 for control over the bandwidth and center frequency. It can be

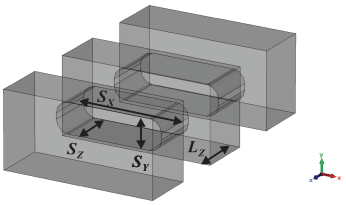

FIGURE 3. A second-order filter structure by mirroring two resonant slot-irises back-to-back. Waveguide structures are WR-10.

clearly shown that the center frequency and bandwidth can be controlled with variations of either the S_X or S_Y dimensions from Fig. 3, respectively. This instance demonstrates the effect of a well controlled filtering response through the use of sequential resonant slot-irises and can be applied to more complex structures, as will be shown in the following sections.

III. TM DUAL-MODE FILTERS

Dual-mode filters using TM and nonresonating modes have been well defined and demonstrated in many works such as [10] and [19]. A short review of the theory and general operation will be discussed here as this work aims to be an improved and alternate approach that ultimately reduces the fabrication complexity and the need for cascading multiple TM-mode cavities as demonstrated in the works previously discussed.

Initially, the fundamental design of the TM dual-mode cavity follows the well-known design equations

$$f_{120} = \frac{c}{2\pi}\sqrt{\left(\frac{\pi}{w}\right)^2 + \left(\frac{2\pi}{h}\right)^2} \tag{1a}$$

$$f_{210} = \frac{c}{2\pi}\sqrt{\left(\frac{2\pi}{w}\right)^2 + \left(\frac{\pi}{h}\right)^2} \tag{1b}$$

from [26], where w = width and h = height of the cavity. In general, the length of the cavity is kept smaller than a quarter of the guided wavelength due to the possible interference of the TE101 mode resonating near the passband of interest. The addition of stepped-corners allow for the formation of the TM120 and TM210 modes within the dual-mode resonant cavity while simultaneously allowing for the nonresonating TM11 mode to act as a source/load bypass coupling. However, one of the key differences in the structure that we propose in this work, is a modification to both of the coupling irises that are connected to the source/load. In this manner the typical thin coupling irises are replaced by resonating slot-irises that were previously described in Fig. 1(b). With this modification, the order of the filter is increased and effectively increases the rejection characteristics above and below the passband. Additionally, by reconfiguring one of the ports from its typical location (as shown in Fig. 5(a)) to the opposite side of TM-mode the cavity (as shown in Fig. 5(b)), and redefining the dimensions, a modified response can be

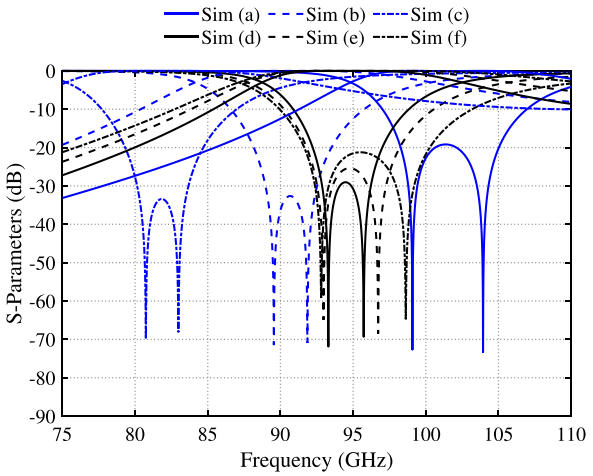

FIGURE 4. Simulated S-parameter results of the slot-iris type resonators shown in Fig. 3 with various values of S_X and S_Y, while S_Z and L_Z are held constant at 0.800 mm and 0.900 mm, respectively. Simulation values are (a) $S_X = 0.800$ mm, $S_Y = 0.231$ mm, (b) $S_X = 0.900$ mm, $S_Y = 0.231$ mm, (c) $S_X = 1.000$ mm, $S_Y = 0.231$ mm, (d) $S_X = 0.861$ mm, $S_Y = 0.200$ mm, (e) $S_X = 0.861$ mm, $S_Y = 0.250$ mm, (f) $S_X = 0.861$ mm, $S_Y = 0.300$ mm.

expressed where, again, there is a significant change to the rejection characteristics. The configurations from Fig. 5 will be refereed to as *configuration (a)*, and *configuration (b)* for simplicity. It is clear that in configuration (b), both of the source/load waveguide ports share a common corner of the TM-mode cavity that is not interrupted by one of the two necessary stepped-corners. A prospective view of this configuration is shown with integrated resonant slot-irises in Fig. 6. It is important to note that a simple mirroring of the port in configuration (a) to configuration (b) will not satisfy the S-parameter goals, re-dimensioning is necessary to stimulate the transmission zero response.

The evolution of the commonly used topology (e.g., [9]) to the new topology containing resonant slot-irises is described in Fig. 7(a) and (b), respectively. The addition of the two resonant slot-irises can facilitate two new poles within the passband while simultaneously acting as a typical coupling iris that allows for the nonresonating TM11 mode to act as a bypass between the first and fourth resonators (now resonating irises) and again on through to the source/load, effectively promoting the formation of two transmission zeros around the passband. Interestingly, the length of the slot irises have little effect on the position of the transmission zeros and simply allow for the bypass coupling to be passed over resonator 2 and 3; a demonstration on the effect of reducing the resonant slot-iris's length is further described in Section IV in order to highlight this effect. In light of the resonant slot-iris topology described in Fig. 7, it will be evident that for a comparison of single-cavity TM-mode cases (i.e., typical second-order versus the proposed fourth-order) that the proposed design achieves better rejection characteristics, better insertion loss, and can overcome narrow bandwidth limitations. Furthermore, a second dual-mode cavity and interconnecting coupling mechanism (such as a thick coupling

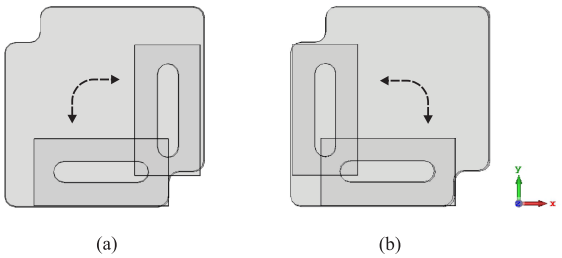

FIGURE 5. Front view of the dual-mode filters. Configuration (a) with typical feed positions (e.g., [10]), and Configuration (b) with a reconfigured coupling location. WR-10 waveguides are shown in each as the feeding ports and centered with respect to the selected irises.

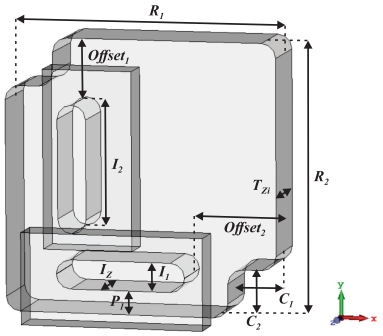

FIGURE 6. Perspective view of the dual-mode filter (configuration (b)) with given design parameters. WR-10 waveguides are centered with respect to the coupling slot-irises. Dimensional values for the fabricated prototype: $R_1 = R_2 = 3.816$ mm, $T_{Zi} = 1.000$ mm, $I_1 = 0.404$ mm, $I_2 = 1.804$ mm, $I_Z = 0.868$ mm, $Offset_1 = Offset_2 = 1.076$ mm, $P_1 = 0.477$ mm, $C_1 = C_2 = 0.678$ mm. All radii are set to 0.200 mm.

slot, quarter-wave waveguide section, or thin coupling slot) that is typically required in the cascaded fourth-order design [9], [10] can be forgone; ultimately allowing for reduced design complexity and a simpler milling procedure.

In previous works of this type, no equations have been outlined, nor is it evident how to easily evaluate this type of structure with resonant irises without the use of extraction tools. In regards to the structure shown in Fig. 6, we propose that a combination of coupling coefficient methods can be used to describe the coupling nature between the symmetric and asymmetric portions of the filter. In this manner, the structure can be evaluated based on the external quality factor Q_e and coupling coefficient $k_{23} = k_{sym}$ which follow from the standard equations [27] as

$$Q_e = \frac{\pi \cdot f_\tau \cdot \tau_{S_{11}}(f_\tau)}{2} \tag{2}$$

$$k_{sym} = \pm \frac{f_1^2 - f_2^2}{f_1^2 + f_2^2}, \tag{3}$$

where τ and f_τ are the S_{11} group delay and its associated center frequency with respect to the first resonator, and f_i for $i = 1, 2$ are the eigenmode frequencies of two symmetric resonators, and the coupling coefficients $k_{12} = k_{34} \approx k_{asym}$ follow from an asymmetric approximation of coupled resonators (in this case, resonator to resonant iris) as

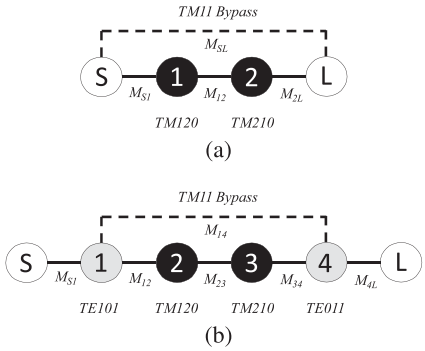

FIGURE 7. Topology evolution: (a) the topology path of a typical dual-mode filter (e.g., [10]), and (b) the topology path of the resonant slot-iris dual-mode dual-band filter. (Resonating nodes are black, source/load nodes are white, and gray nodes are resonating slot-irises. Solid lines indicate the direct-coupling paths and dashed lines indicate bypass-coupling paths.).

$$k_a = \pm \frac{f_{1a}^2 - f_{2a}^2}{f_{1a}^2 + f_{2a}^2} \tag{4a}$$

$$k_b = \pm \frac{f_{1b}^2 - f_{2b}^2}{f_{1b}^2 + f_{2b}^2} \tag{4b}$$

$$k_{asym} \approx \pm \sqrt{|k_a \cdot k_b|}, \tag{4c}$$

where f_{ix} for $i = 1, 2$ and $x = a, b$ are the eigenmode frequencies of two symmetric resonators formed from the mirroring of two decoupled asymmetric resonators [28], [29].

In the case of the TM11 bypass coupling, we propose a modified approach to the method described by [5] for TM110-mode filters; this approach can be used to approximate the $k_{14} = k_{bypass}$ of the proposed filter by removing the stepped corners of the TM-mode cavity and studying the transmission coefficient as

$$k_{bypass} \approx \pm \frac{1 - \sqrt{1 - |S_{21,SL}|^2}}{S_{21,SL}}, \tag{5}$$

where $|S_{21,SL}|$ is the transmission coefficient of the source/load coupling through the TM-mode cavity [5], [30]. In this manner, the structures in Figs. 5 and 6 can be defined by coupling matrix theory.

IV. FILTER CONFIGURATIONS AND ATTRIBUTES

In order to demonstrate the functional nature of the proposed topology, a dimensional analysis is exhibited for simulated filters operating at 90 GHz with varying fractional bandwidths as well as a prototype filter to be fabricated for operation at 90 GHz with a fractional bandwidth of approximately 7.3%.

Fig. 8 depicts the S-parameter responses of filter configuration (a) with and without resonant slot-irises. It can be shown that for similar specifications where the transmission zeros are held at the same locations, a significant improvement can be rendered over the full frequency band in favour of the resonant-iris type TM-mode filter structure. In a similar manner, configuration (a) and (b) are compared in Fig. 9 with similar dimensions and similar specified bandwidths.

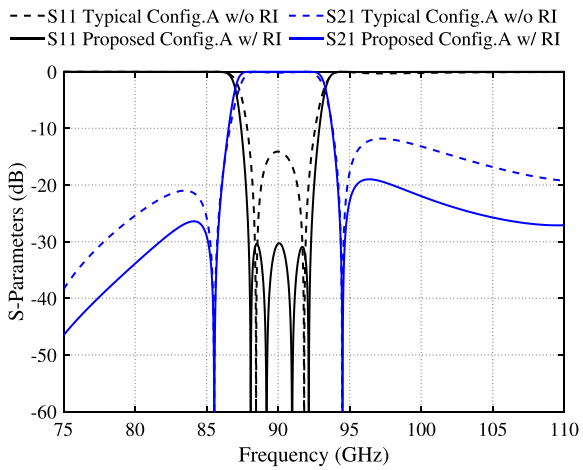

FIGURE 8. The simulated S-parameters of a typical TM dual-mode filter [10] (Configuration (a) without resonant slot-irises) versus the proposed TM dual-mode filter (Configuration (a) with resonant slot-irises). The transmission zeros are held in the same position for a relative comparison between the second- and fourth-order characteristics.

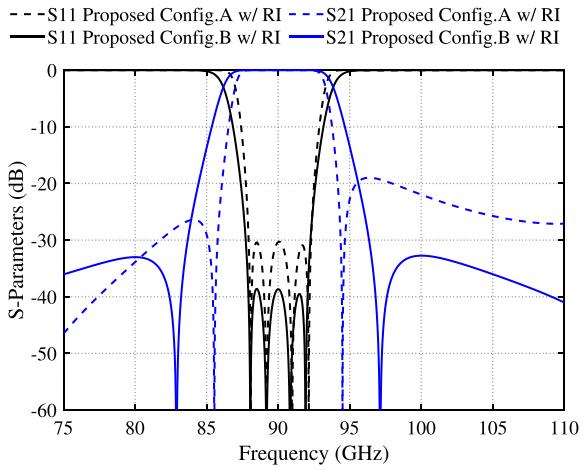

FIGURE 9. The simulated S-parameters of the proposed TM dual-mode filter (Configuration (a) with resonant slot-irises) and its reconfigured version (Configuration (b) with resonant slot-irises). The 20 dB bandwidth is held in approximately the same position for a relative comparison between the return loss improvement and detuning of the transmission zero locations for filters with similar dimensions.

Observing the differences in transmission zero location, it is clear that the bypass coupling value is altered by changing from configuration (a) to (b), and the achievable rejection region characteristics are effected, particularly in the upper portion of the frequency band, and the return loss is further improved. Although comparisons generally maintain equivalent characteristics such as filter order and return loss ripple, this comparison highlights the evident improvements with minimal dimensional variation and similar bandwidth requirements.

Utilizing configuration (b) for its strong quasi-elliptic response, a filter operating at 90 GHz with a fractional bandwidth of approximately 7.3% is demonstrated and analyzed;

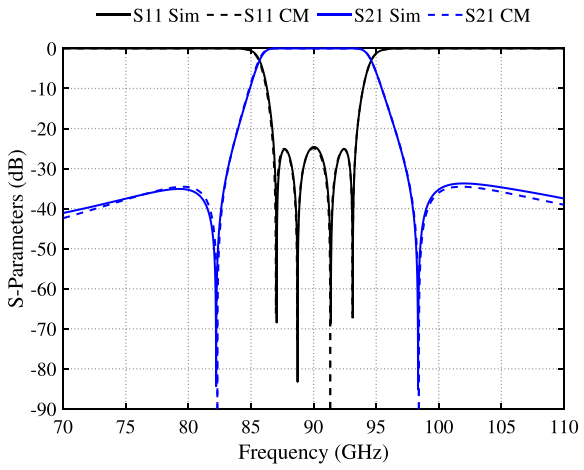

FIGURE 10. Simulated narrowband ($FBW = 7.3\%$) S-parameter response of the TM-mode filter in Configuration (b) with resonant slot-irises and its associated coupling matrix S-parameters from equation (6). The filter dimensions are specified in Fig. 6.

first, with respect to the effects of parameter variations on the coupling values, and then the S-parameter characteristics with respect to dimensional variations in the lengths of both of the resonant slot-irises and the TM-mode resonator length itself. Fig. 10 depicts the simulated S-parameter response, where the coupling matrix response, described by (6), follows from equations (1)–(5) with regards to the filter structure defined in Fig. 6; note that the internal radii of corners is specified as 0.2 mm. Fig. 11(a) and (b) demonstrate the effects of parameter variation on the external quality factor, coupling values and resonant-iris frequency. Each parameter is swept over a wide range in order to highlight the effects.

$$\begin{bmatrix} 0 & 1.140 & 0 & 0 & 0 & 0 \\ 1.140 & 0 & 1.002 & 0 & -0.157 & 0 \\ 0 & 1.002 & 0 & 0.824 & 0 & 0 \\ 0 & 0 & 0.824 & 0 & 1.002 & 0 \\ 0 & -0.157 & 0 & 1.002 & 0 & 1.140 \\ 0 & 0 & 0 & 0 & 1.140 & 0 \end{bmatrix}. \quad (6)$$

Control over the length of the resonant slot-iris dimension I_Z is demonstrated in Fig. 12 for the structure and given dimensions outlined in Fig. 6. Studying Fig. 12, stimulation of two additional poles can be seen within the passband while varying the dimension I_Z over the range of $I_Z = 0.1$ mm to 0.868 mm. Inspection of this response sequence shows that a variation in the length of irises has negligible effect on the position of the transmission zeros. However, the bandwidth and selectivity of the filter is substantially increased, where on comparison of Fig. 12(a) and (f), the lowest rejection level at the edges of the plots can be shown to evolve from approximately 20 dB to 36 dB, while the return loss ripple evolves from approximately 1.8 GHz bandwidth at 36 dB to approximately 6.5 GHz bandwidth at 25 dB, demonstrating

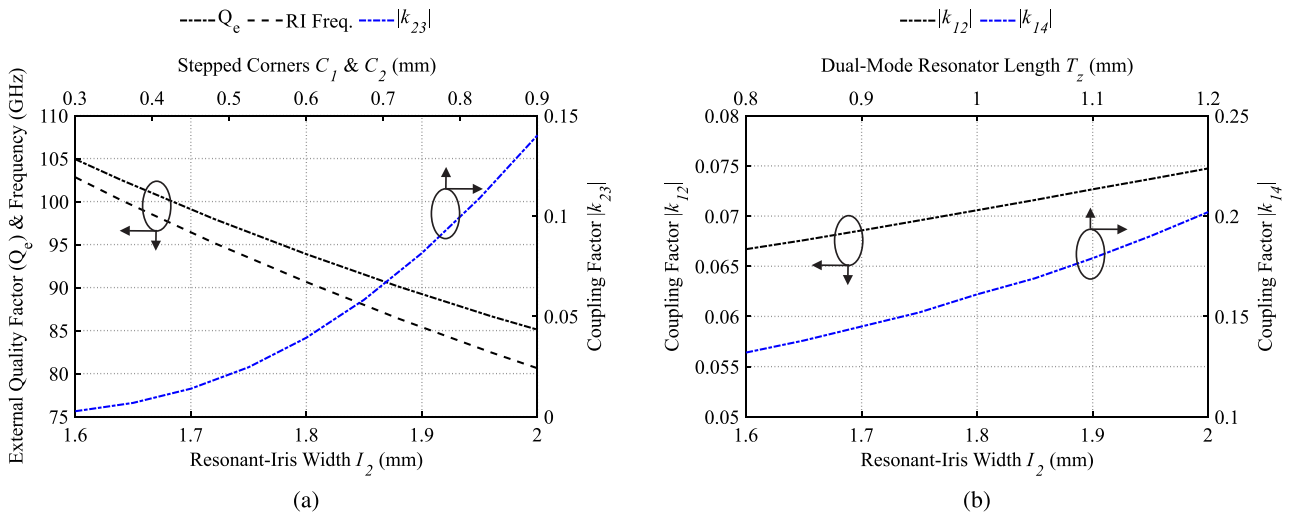

FIGURE 11. **Effects of parameter variation on the external quality factor, coupling values and resonant-iris frequency for the filter specified in Fig 6. (a) External quality factor, resonant-iris frequency, and coupling factor k_{23}'s dependence on resonant-iris width I_2 and stepped corner sizes C_1 and C_2, and (b) Coupling factor k_{12} and k_{14}'s dependence on resonant-iris width I_2 and the dual-mode resonator length T_Z.**

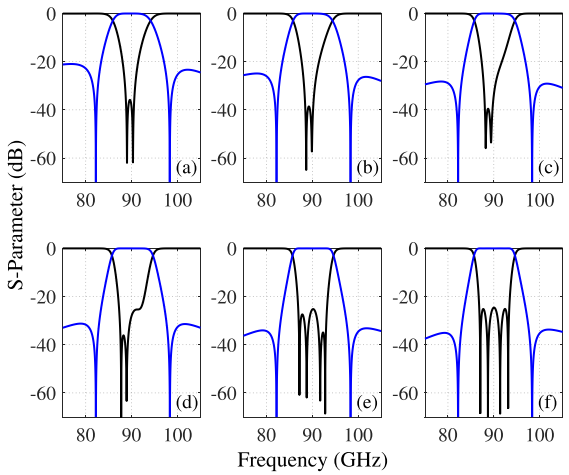

FIGURE 12. **Evolution of the simulated S-parameter response for the proposed dual-mode filter specified in Fig. 6 while varying the resonant slot-iris thickness value (I_Z). For images (a) though (f), $I_Z = 0.1$ mm, 0.275 mm, 0.45 mm, 0.625 mm, 0.8 mm, and 0.868 mm respectively. (re-optimized dimensions not shown).**

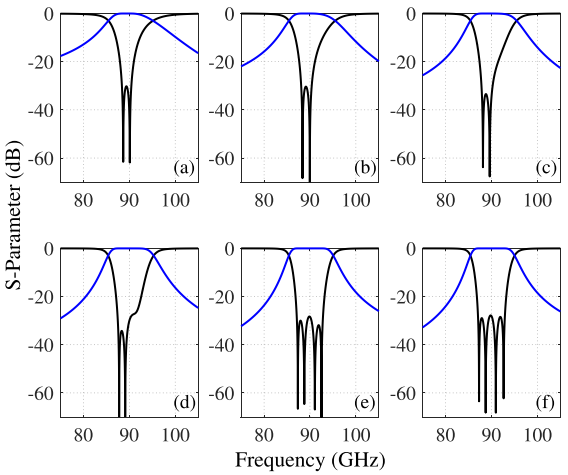

FIGURE 13. **Evolution of the simulated S-parameter response for the proposed dual-mode filter specified in Fig. 6 when one of the ports is mirrored across the TM-mode cavity for equalized filter characteristics. The resonant slot-iris thickness value (I_Z) is again varied. For images (a) though (f), $I_Z = 0.1$ mm, 0.275 mm, 0.45 mm, 0.625 mm, 0.8 mm, and 0.868 mm respectively. (re-optimized dimensions not shown).**

a substantial variation of the characteristic response with respect to parameter I_Z.

In regards to the simple mirroring of one of the source/load feeding ports to the opposite side of the TM-mode cavity (and with minimal re-dimensioning), a coupling sign change is invoked which results in an all-pole equalized filter response. This case is shown in Fig. 13, where a mirroring of one of the feed ports back to configuration (a) and a re-optimization of the dimensions is applied. In this scenario, the characteristics of a fourth-order Chebyshev response can be shown, where again, the stimulation of the two resonant slot-irises can be seen within the passband while varying the resonant slot-iris length from $I_Z = 0.1$ mm to 0.868 mm. Again the bandwidth and selectivity of the filter is substantially increased with the use of the resonant slot-irises, where on comparison of Fig. 13(a) and (f), the lowest rejection level at the edges of the plots can be shown to evolve from approximately 16.4 dB to 25.7 dB, while the return loss ripple evolves from approximately 2.1 GHz bandwidth at 30 dB to approximately 5.9 GHz bandwidth at 28 dB. Again, demonstrating a substantial variation of the characteristic response with respect to parameter I_Z. In order to control the transmission zero response, a variation of the TM-mode cavity length (T_{Zi}) can be applied, where in Fig. 14, a demonstration of the transmission zero control is shown over the dimensional range of $T_{Zi} = 0.7$ mm to 1.5 mm.

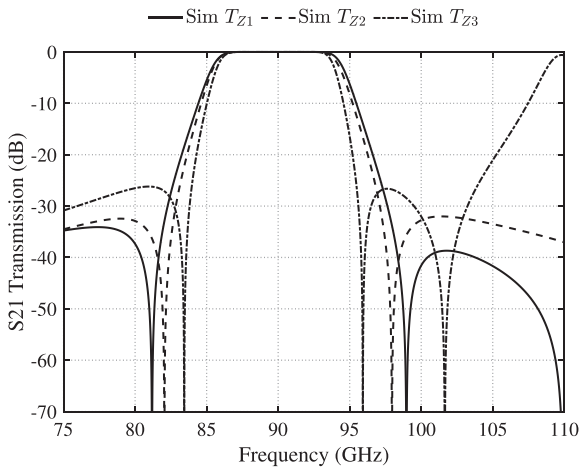

FIGURE 14. Simulated transmission response of the resonant slot-iris dual-mode filter specified in Fig. 6 while varying the dual-mode resonator thickness value (T_{Zi}), where $i = 1, 2, 3$. $T_{Z1} = 0.7$ mm, $T_{Z2} = 1.0$ mm, and $T_{Z3} = 1.5$ mm. (re-optimized dimensions not shown).

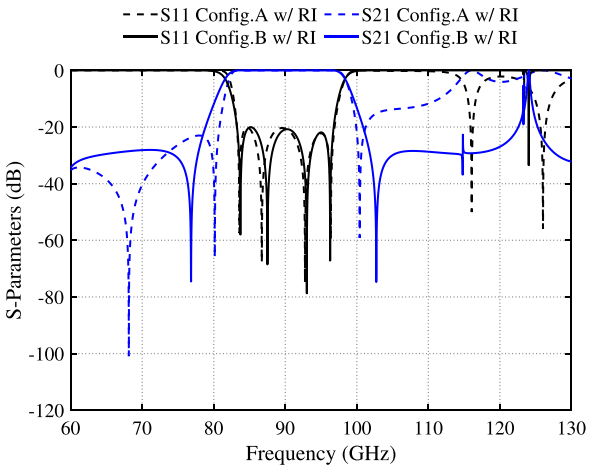

FIGURE 15. Wideband (*FBW* = 15%) simulated S-parameter response of the TM-mode filter in Configuration (a) and Configuration (b) with similar dimensions and both with resonant slot-irises.

In [10], an upper limit of approximately 7% fractional bandwidth is suggested for the TM-mode filter. However, in light of the properties of the new topology proposed in Fig. 7(b), we expand this fractional bandwidth limit by more than double and demonstrate the simulated results to be suitable for at least 15% fractional bandwidth in both configuration (a) and (b). The S-parameter results are shown in Fig. 15 with a similar return loss ripple and fractional bandwidth over 60 GHz to 130 GHz. It can be noted that the achievable fractional bandwidth can be greater 15% and Fig. 15 is used as a wideband example. On the lower limit for a usable narrow fractional bandwidth, a practical limit of 2% is suggested. Notwithstanding, these bounds may be exceeded, however, can come at the cost of undesirable effects such as the introduction of spurious modes and increased losses. For bandwidth below 2%, the use of the classical structure is recommended. The simulated transmission response for the

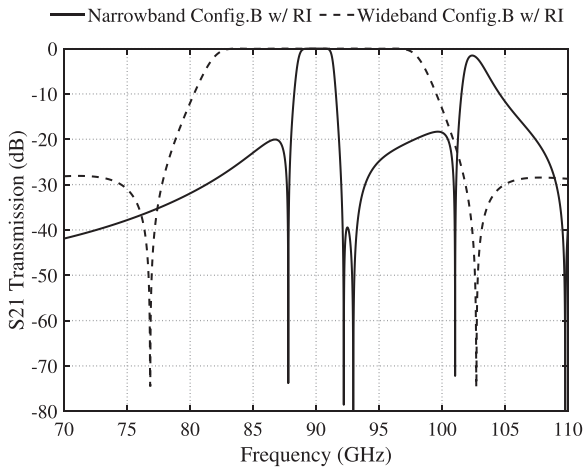

FIGURE 16. Narrowband (*FBW* = 2%) and wideband (*FBW* = 15%) simulated S-parameter responses of the TM-mode filter in Configuration (b), both with resonant slot-irises.

stated practical fractional bandwidth limits are demonstrated in Fig. 16.

V. FABRICATION AND RESULTS

As a demonstration of the compact and simple nature of this design, a prototype filter corresponding to the specifications outlined in the previous section for a 90 GHz filter operating with a 7.3% fractional bandwidth has been manufactured. Brass has been selected as the cutting material due to its machinability and high-quality surface finish in high-precision CNC milling. The dimensions of the structure are defined in Fig. 6 with internal radii of 0.2 mm. Images of the milled cavity and the assembled filter are shown in Fig. 17(a) and Fig. 17(b), respectively. The measured surface roughness of the milled cavity in Fig. 17(a) has been found to be approximately $R_a \approx 1\ \mu m$, where R_a describes the mean arithmetic height.

Once fabricated and assembled, the filter was tested using a Rohde & Schwarz ZVA67 with W-band up-converters. Fig. 18 presents a comparison of the simulated and measured results over 75 GHz to 110 GHz. This direct comparison demonstrates good measured results; the return loss is better than 20 dB, while the insertion loss is on range of 0.42 dB to 0.63 dB throughout the measured passband. Analyzing the response, the unloaded quality factor is found to be approximately $Q_u \approx 550$. The measured results demonstrate very high accuracy when compared to the simulated results in both the passband and rejection regions with negligible shift in center frequency. A close-up view of the simulated and measured insertion loss is given in Fig. 19 over the range of 83 GHz to 97 GHz. No gold (Au) or silver (Ag) coating has been applied to enhance the performance. The results of the prototype allow for the design approach to be demonstrated as a competitive option for ultra-compact structures, especially when selecting structures suitable for millimetre-wave design where tuning screws or the cascading and alignment of multiple cavities becomes increasingly difficult, if not infeasible.

FIGURE 17. **Fabricated W-band prototype. (a) Close-up view of the internal cavity and one of the resonating iris-slots, and (b) the assembled filter unit.**

VI. Q-FACTOR COMPARISON

As a verification of the design methodology, the Q-factor of a proposed configuration (b)-type filter is compared to several other TM-mode filter designs. Although it is evident that not all filtering characteristics can be matched, the two primary attributes in the comparison are in terms of equal return loss ripple and fractional bandwidth. In this comparison, the pass-band is set between 87.2 GHz to 92.8 GHz for a fractional bandwidth of 6.2%. In this manner, the typical dual-mode filter configuration -[9]- is within its suggested upper limit of 7% fractional bandwidth, while the proposed filter is closer to its lower limit.

Three filters are compared to the proposed filter design, two of which are variations of the typical dual-mode filter design – shown in Fig. 20(b) – and one of which is similar to the TM110 single-mode filters demonstrated in [31] – shown in Fig. 20(c). The simulated results of the four filters are shown in Fig. 21 over 70 GHz to 110 GHz. The equivalent conductivity of brass used for the measurement comparison provided in Section V has been applied to each of the structures for a realistic Q-factor comparison. The inset of Fig. 21 provides insight into the capabilities of each of these filters over 82 GHz to 98 GHz, where it can be clearly shown that the proposed filter in this work provides the lowest and flattest insertion loss of the four designs. Table 1 is provided for a quick comparison of values between the specified passband range. Although some argument can be made in regards to the variation of the S_{21} parameters in terms of transmission zeros, spurious modes, and relative selectivity, it can be understood that it is difficult to perfectly match all characteristics, and the authors estimate the Q-factors as best as possible for simulated data for designs with equal return-loss ripple and fractional bandwidth. The proposed filter design reaches a $Q_u \approx 660$, the two typical dual-mode designs reach $Q_u \approx 350$, and the four-cavity single-mode design from Fig. 20(c) reaches $Q_u \approx 350$. It is note worthy to observe that with the use of resonant-irises, the Q-factor of the proposed design still overcomes that of the other simulated structures and provides a very flat insertion loss within the specified passband. Furthermore, the fabrication complexity is kept minimal by only requiring the use of one TM-mode cavity, opposed to two or four cavities that are required by the other design schemes to achieve fourth-order filter characteristics.

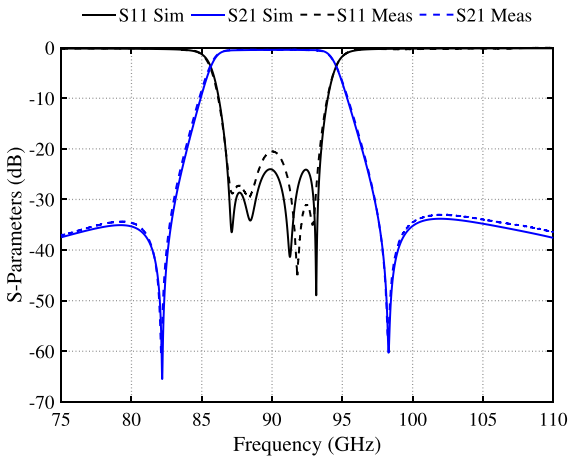

FIGURE 18. **Simulated versus measured S-parameters of the resonant slot-iris dual-mode filter modelled in Fig. 6. (equivalent conductivity of brass taken as $5.9x10^6$ *S/m*).**

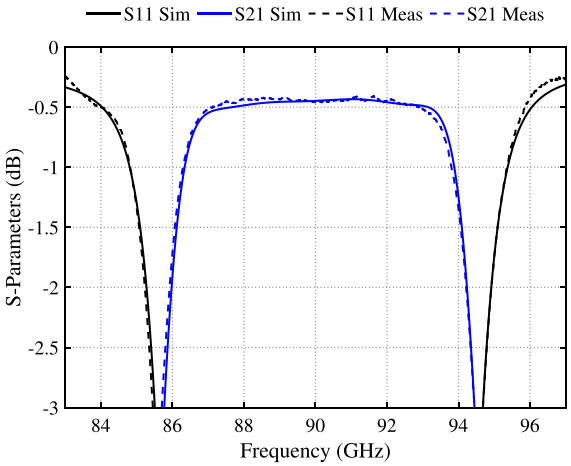

FIGURE 19. **Close-up view of the simulated versus measured insertion loss of the resonating-iris dual-mode filter modelled in Fig. 6. (equivalent conductivity of brass taken as $5.9x10^6$ *S/m*).**

While it may be possible to increase the Q-factor of the structures shown in Fig. 20(b) and (c) by increasing their length, one must take into account that a simple lengthening of the cavities has intrinsic effects; primarily, the transmission zero positions will be altered due to a variation of the bypass coupling. In order to compensate this effect, one must try to vary the other dimensions of the filter, often resulting in other undesirable trade-offs that do not meet the required specifications. This becomes especially difficult if one considers that the length of the cavity should remain smaller than a quarter of the guided wavelength to keep the TE101 mode from resonating in the vicinity of the passband. Moreover, from a fabrication complexity point of view, the additional parts that are required to assemble the classical designs will cause more gaps, dimensional errors and misalignments that further degrade the Q-factor performance when applied in practice.

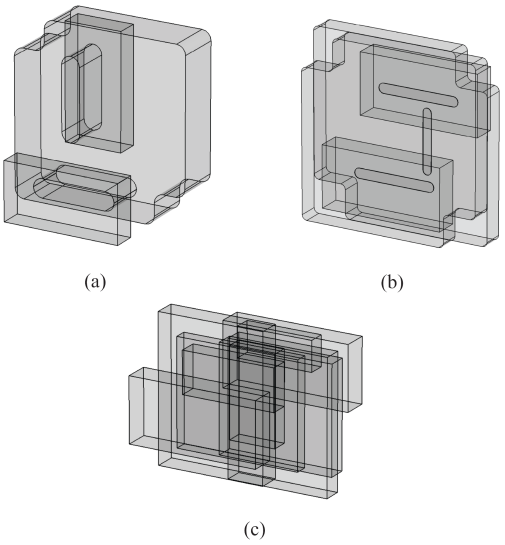

FIGURE 20. Fourth-order TM-mode filter structures. (a) The proposed dual-mode TM-mode resonant-iris filter structure, (b) the typical dual-mode TM-mode filter structure [10], and a single-mode (TM110) four-cavity structure [31].

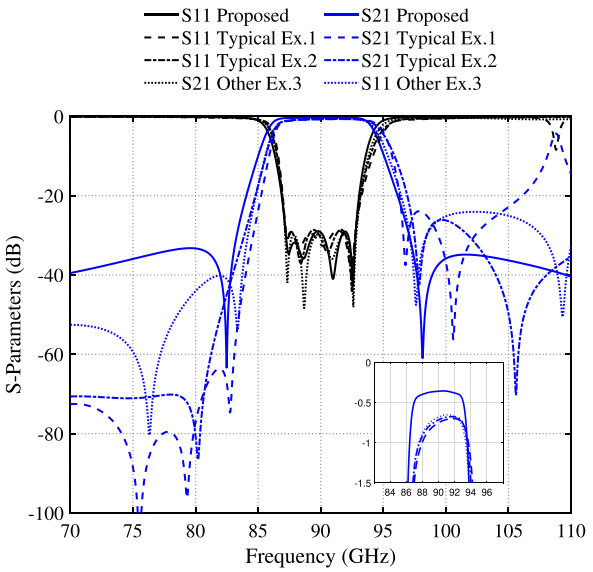

FIGURE 21. Simulated S-parameters of fourth-order single- and dual-TM-mode filters with $FBW = 6.2\%$. The proposed dual-mode filter takes the form of Fig. 20(a), dual-mode examples (Ex.1 and Ex.2) take the form of Fig. 20(b), and the single-mode example (Ex.3) takes the form of Fig. 20(c). (equivalent conductivity of all filters is taken as $5.9x10^6$ S/m).

TABLE 1. Comparison of Simulated Fourth-Order TM-Mode Filters Operating at 90 GHz and 6.2% FBW

Filter‡	TM-mode Cavities (#)	IL (dB)	Approx. Q-factor	Design Style (from Fig.20)
Proposed	1	0.45 - 0.36	660	(a)
Ex.1	2	1.31 - 0.70	350	(b)
Ex.2	2	1.17 - 0.68	350	(b)
Ex.3	4	1.17 - 0.66	350	(c)

‡The equivalent conductivity of brass is taken as $5.9x10^6$ S/m for all filters.

VII. CONCLUSION

In this work, an alternate and improved approach for the design of dual-mode filters that utilize TM and nonresonating modes has been investigated. A reconfiguration of the typical TM dual-mode design allows for the inclusion of resonant irises between the TM-mode cavity and the source/load connections. This approach demonstrates an improvement to the typical single-cavity design in several aspects, that being: increased filter order and suitability for wideband and millimetre-wave frequencies, all with minimal alterations to the original design, while in comparison to equal-order designs, a reduction in fabrication complexity and improved insertion loss is achieved. Furthermore, this method designates all of the filter's structural elements with a minimum of two operating purposes or modes in order to optimize the given geometry. In this manner, the novelty of the filter approach presented in this work allows for simple, compact and lightweight designs which do not require any tuning elements. A prototype of a W-band fourth-order quasi-elliptic filter has been manufactured using high-precision CNC milling in order to demonstrate the elegance and reduced complexity of the design. The prototype has been tested and demonstrates an exceptionally accurate response over the full frequency band of interest. A comparison of simulated fourth-order TM-mode filters is provided in order to highlight the obtainable Q-factor and flatness of the insertion loss with respect to other filter types, ultimately validating the design approach.

REFERENCES

[1] S. Amari, U. Rosenberg, and J. Bornemann, "Singlets, cascaded singlets, and the nonresonating node model for advanced modular design of elliptic filters," *IEEE Microw. Wireless Compon. Lett.*, vol. 14, no. 5, pp. 237–239, May 2004.

[2] S. Amari and U. Rosenberg, "The doublet: A new building block for modular design of elliptic filters," in *Proc. 32nd Eur. Microw. Conf.*, Milan, Italy, 2002, pp. 1–3.

[3] U. Rosenberg and S. Amari, "Novel design possibilities for dual-mode filters without intracavity couplings," *IEEE Microw. Wireless Compon. Lett.*, vol. 12, no. 8, pp. 296–298, Aug. 2002.

[4] M. Bekheit and S. Amari, "A direct design technique for dual-mode inline microwave bandpass filters," *IEEE Trans. Microw. Theory Techn.*, vol. 57, no. 9, pp. 2193–2202, Sep. 2009.

[5] U. Rosenberg, S. Amari, and J. Bornemann, "Inline TM/sub 110/-mode filters with high-design flexibility by utilizing bypass couplings of nonresonating TE/sub 10/01/ modes," *IEEE Trans. Microw. Theory Techn.*, vol. 51, no. 6, pp. 1735–1742, Jun. 2003.

[6] U. Rosenberg, S. Amari, and J. Bornemann, "Mixed-resonance compact in-line pseudo-elliptic filters," in *IEEE MTT-S Int. Microw. Symp. Dig.*, Philadelphia, PA, USA, 2003, pp. 479–482.

[7] C. Bartlett and M. Höft, "Dual-mode dual-band bandpass filter design utilising cylindrical TM-mode cavities," *Electron. Lett.*, vol. 57, no. 8, pp. 328–330, 2021.

[8] S. Bastioli, L. Marcaccioli, C. Tomassoni, and R. Sorrentino, "Ultra-compact highly-selective dual-mode pseudoelliptic filters," *IET Electron. Lett.*, vol. 46, no. 2, pp. 147–149, Jan. 2010.

[9] S. Bastioli, C. Tomassoni, and R. Sorrentino, "A new class of waveguide dual-mode filters using TM and nonresonating modes," *IEEE Trans. Microw. Theory Techn.*, vol. 58, no. 12, pp. 3909–3917, Dec. 2010.

[10] S. Bastioli, "Nonresonating mode waveguide filters," *IEEE Microw. Mag.*, vol. 12, no. 6, pp. 77–86, Oct. 2011.
[11] S. Bastioli and R. V. Snyder, "Quasi-elliptic evanescent-mode filters using non-resonating mode waveguide cavities," *Int. J. Microw. Wireless Techn.*, vol. 7, no. 3/4, pp. 211–218, Feb. 2015.
[12] C. Tomassoni, S. Bastioli, and R. Sorrentino, "Generalized TM dual-mode cavity filters," *IEEE Trans. Microw. Theory Techn.*, vol. 59, no. 12, pp. 3338–3346, Dec. 2011.
[13] S. C. Mejillones, M. Oldoni, S. Moscato, and G. Macchiarella, "Analytical synthesis of fully canonical cascaded-doublet prototype filters," *IEEE Microw. Wireless Compon. Lett.*, vol. 30, no. 11, pp. 1017–1020, Nov. 2020.
[14] L. Pelliccia et al., "Very-compact waveguide bandpass filter based on dual-mode TM cavities for satellite applications in Ku-band," in *Proc. 48th Eur. Microw. Conf.*, Madrid, Spain, 2018, pp. 93–96.
[15] V. Nocella, F. Cacciamani, C. Tomassoni, R. Sorrentino, and L. Pelliccia, "Dual-band filters based on TM dual-mode cavities," in *Proc. 44th Eur. Microw. Conf.*, Rome, Italy, 2014, pp. 179–182.
[16] C. Tomassoni, M. Dionigi, and R. Sorrentino, "Strategies for the improvement of the out of band behavior of TM dual-mode filters," in *Proc. IEEE 1st Int. Forum Res. Techn. Soc. Ind. Leveraging a Better Tomorrow*, Turin, Italy, 2015, pp. 90–93.
[17] S. Bastioli and R. V. Snyder, "Stubbed waveguide cavity filters," *IEEE Trans. Microw. Theory Techn.*, vol. 67, no. 12, pp. 5049–5060, Dec. 2019.
[18] Q. Liu, D. Zhou, D. Lv, D. Zhang, and Y. Zhang, "Ultra-compact highly selective quasi-elliptic filters based on combining dual-mode SIW and coplanar waveguides in a single cavity," *IET Microw., Antennas Propag.*, vol. 12, no. 3, pp. 360–366, Mar. 2018.
[19] S. Bastioli and R. V. Snyder, "Nonresonating modes do it better!: Exploiting additional modes in conjunction with operating modes to design better quality filters," *IEEE Microw. Mag.*, vol. 22, no. 1, pp. 20–45, Jan. 2021.
[20] U. Rosenberg, S. Amari, J. Bornemann, and R. Vahldieck, "Compact pseudo-highpass filters formed by cavity and iris resonators," in *Proc. 34th Eur. Microw. Conf.*, Amsterdam, The Netherlands, 2004, pp. 985–988.
[21] J. F. Valencia Sullca, S. Cogollos, M. Guglielmi, and V. E. Boria, "Dual-band filters in rectangular waveguide based on resonant apertures," in *IEEE MTT-S Int. Microw. Symp. Dig.*, Atlanta, GA, USA, 2021, pp. 192–195.
[22] C. Zong-tao and L. Sheng-xian, "Design of microwave filter with resonant irises of resonant windows at different location," in *Proc. IEEE Int. Conf. Microw. Techn. Compon. Electromagn.*, Beijing, China, 2011, pp. 156–159.
[23] T.-S. Chen, "Characteristics of waveguide resonant-iris filters," *IEEE Trans. Microw. Theory Techn.*, vol. 15, no. 4, pp. 260–262, Apr. 1967.
[24] R.-M. Barrio-Garrido, S. Llorente-Romano, and M. Salazar-Palma, "Design of Ka band highly selective wideband band-pass filters using directly coupled resonant irises," in *IEEE Antennas Propag. Soc. Int. Symp. Dig.*, vol. 2. Columbus, OH, USA, 2003, pp. 1161–1164.
[25] R.-M. Barrio-Garrido, S. Llorente-Romano, A. Garcia-Lamperez, and M. Salazar-Palma, "Design of broadband directly coupled non-centred resonant irises filters," in *Proc. 33rd Eur. Microw. Conf.*, Munich, Germany, 2003, pp. 219–222.
[26] D. M. Pozar, *Microwave Engineering*, 4th ed. Hoboken, NJ, USA: Wiley, 2011.
[27] J.-S. Hong and M. J. Lancaster, *Microstrip Filters for RF/Microwave Applications*. New York, NY, USA: Wiley, 2001.
[28] J.-F. Liang, K. Zaki, and A. Atia, "Mixed modes dielectric resonator filters," *IEEE Trans. Microw. Theory Techn.*, vol. 42, no. 12, pp. 2449–2454, Dec. 1994.
[29] A. R. Harish and J. S. K. Raj, "A direct method to compute the coupling between nonidentical microwave cavities," *IEEE Trans. Microw. Theory Techn.*, vol. 52, no. 12, pp. 2645–2650, Dec. 2004.
[30] M. Ohira, H. Aoyama, and Z. Ma, "Deterministic extraction of direct source/load coupling and its application to multi-mode filter designs based on transversal array network theory," in *IEEE MTT-S Int. Microw. Symp. Dig.*, Seattle, WA, USA, 2013, pp. 1–4.
[31] J. Bornemann, U. Rosenberg, S. Amari, and R. Vahldieck, "Tolerance analysis of bypass-, cross-, and direct-coupled rectangular waveguide band-pass filters," *Inst. Elect. Eng. Proc., Microw., Antennas, Propag.*, vol. 152, no. 3, pp. 167–170, Jun. 2005.

CHAD BARTLETT (Graduate Student Member, IEEE) was born in Nelson, BC, Canada, in 1987. He received the B.Eng. and MA.Sc. degrees in electrical engineering from the University of Victoria, Victoria, BC, Canada, in 2017 and 2019, respectively. He is currently working toward the Dr.-Ing. degree with the Chair of Microwave Engineering, Institute of Electrical and Information Engineering, University of Kiel, Kiel, Germany, and is a Member of the European Union's Horizon 2020 research and innovation programme for early-stage researchers. His research interests include microwave and millimeter-wave passive components, filters and antenna networks for the next generation of satellite and communication systems, and developing methods for overcoming challenges in micro-scale designs.

JENS BORNEMANN (Life Fellow, IEEE) received the Dipl.-Ing. and Dr.-Ing. degrees in electrical engineering from the University of Bremen, Bremen, Germany, in 1980 and 1984, respectively. From 1984 to 1985, he was an Engineering Consultant. In 1985, he joined the University of Bremen, Germany, as an Assistant Professor. Since April 1988, he has been with the Department of Electrical and Computer Engineering, University of Victoria, Victoria, BC, Canada, where he became a Professor in 1992. From 1992 to 1995, he was a Fellow of the British Columbia Advanced Systems Institute. In 1996, he was a Visiting Scientist with Spar Aerospace Limited (now MDA Space), Ste-Anne-de-Bellevue, Quebec, Canada, and a Visiting Professor with the Microwave Department, University of Ulm, Ulm, Germany. From 1997 to 2002, he was a Co-Director of the Center for Advanced Materials and Related Technology, University of Victoria. From 1999 to 2002, he was an Associate Editor for IEEE TRANSACTIONS ON MICROWAVE THEORY AND TECHNIQUES in the area of Microwave Modeling and CAD. From 2006 to 2008, he was an Associate Editor for the *International Journal of Electronics and Communications*. In 2003, he was a Visiting Professor with the Laboratory for Electromagnetic Fields and Microwave Electronics, ETH Zurich, Switzerland. From 1999 to 2009, he was on the Technical Program Committee of the IEEE MTT-S International Microwave Symposium. He has coauthored *Waveguide Components for Antenna Feed Systems - Theory and Design* (Artech House, 1993) and has authored or coauthored more than 350 technical papers. His research activities include RF/wireless/microwave/millimeter-wave components and systems design, and field-theory-based modeling of integrated circuits, feed networks and antennas. He is a Registered Professional Engineer with the Province of British Columbia, Canada. He is a Fellow of the Canadian Academy of Engineering and the Engineering Institute of Canada, and he is on the Editorial Advisory Board of the *International Journal of Numerical Modelling*.

MICHAEL HÖFT (Senior Member, IEEE) was born in Lübeck, Germany, in 1972. He received the Dipl.-Ing. degree in electrical engineering and the Dr.-Ing. degree from the Hamburg University of Technology, Hamburg, Germany, in 1997 and 2002, respectively. From 2002 to 2013, he was with the Communications Laboratory, European Technology Center, Panasonic Industrial Devices Europe GmbH, Lüburg. He was a Research Engineer and then a Team Leader, where he had been engaged in research and development of microwave circuitry and components, particularly filters for cellular radio communications. From 2010 to 2013, he was a Group Leader of research and development of sensor and network devices. Since October 2013, he has been a Full Professor with the Faculty of Engineering, University of Kiel, Kiel, Germany, where he currently heads the Chair of Microwave Engineering, Institute of Electrical and Information Engineering. His research interests include active and passive microwave components, submillimeter-wave quasioptical techniques and circuitry, microwave and field measurement techniques, microwave filters, microwave sensors, and magnetic field sensors. He is a member of the European Microwave Association, the Association of German Engineers, and the German Institute of Electrical Engineers.